Journal of Solid State Chemistry **145,** 235–246 (1999)
Article ID jssc.1999.8257, available online at http://www.idealibrary.com on IDEAL®

Evidences for the Formation of Chromium in the Unusual Oxidation State Cr(IV)

II. Magnetic Properties and Low-Temperature X-Ray Investigations of the Nonstoichiometric Channel Compounds $Tl_xCr_5Se_8$ ($0 \leq x \leq 1$)

Wolfgang Bensch, Bernd Sander, Oliver Helmer, and Christian Näther

Institut für Anorganische Chemie, Universität Kiel, Olshausenstr. 40, D-24098 Kiel, Germany

Felix Tuczek

Institut für Anorganische und Analytische Chemie, Universität Mainz, Staudingerweg 9, D-55099 Mainz, Germany

and

Alexander I. Shames and Alexander M. Panich

Department of Physics, Ben-Gurion University of the Negev, P.O. Box 653, 84 105 Be'er-Sheva, Israel

Received August 6, 1998; in revised form March 3, 1999; accepted March 10, 1999

Magnetic measurements on $Tl_xCr_5Se_8$ ($0 \leq x \leq 1$) reveal that stoichiometric $TlCr_5Se_8$ is a three-dimensional antiferromagnet with a Néel temperature T_N of about 55 K. In contrast, samples with a reduced Tl content show highly unusual magnetic properties that are without precedent in the literature of magnetically coupled systems: upon lowering the temperature from 300 K the susceptibility reaches a maximum at about 125 K and then steeply drops to a value comparable to that obtained at room temperature. The height of this maximum increases first with decreasing Tl abundance reaching its largest value at a composition $Tl_{0.2}Cr_5Se_8$ and then decreases again for samples with $x < 0.2$. With decreasing Tl content the effective magnetic moment per Cr^{3+} decreases, indicating the successive formation of Cr^{4+} ($3d^2$) centers. For samples $Tl_xCr_5Se_8$ with $x > 0.5$ the predominant magnetic exchange is antiferromagnetic and becomes ferromagnetic for $x < 0.5$. The magnetic data suggest a very similar spin structure for all samples except $TlCr_5Se_8$ below about 125 K. Low-temperature single-crystal X-ray investigations on $Tl_xCr_5Se_8$ ($x = 0.5$ and 0.32) show a thermal expansion anomaly of the unit cell volume as well as of the b-axis starting at about 125 K, which is accompanied by an enlargement of one of the three Cr–Cr interatomic distances. The anomalous thermal behavior of the lattice parameters reflects competing antiferromagnetic and ferromagnetic exchange interactions. Detailed analysis of the Cr–Cr distances as a function of temperature gives evidence that the positive charge associated with the formation of Cr(IV) is delocalized between two chromium atoms at higher temperatures and trapped upon cooling on one Cr site. The localization of Cr(IV) centers induces net antiferromagnetic coupling. EPR investigations are in agreement with this picture. They show that in stoichiometric $TlCr_5Se_8$ the Cr^{3+} centers are antiferromagnetically coupled. For Tl-poor samples, the temperature dependence of g_{eff} follows the susceptibility curve, increasing upon cooling and passing a maximum at about 130 K. © 1999 Academic Press

INTRODUCTION

In our previous contribution we reported on the preparation, microhomogeneity, and X-ray investigations of metastable samples of $Tl_xCr_5Se_8$ ($0 \leq x < 1$) (1). The crystal structure of $TlCr_5Se_8$ is built up of $CrSe_6$ octahedra sharing edges and faces to form channels running parallel to the crystallographic *b* axis. The Tl atoms are confined within these channels (Fig. 1a). The connection of the $CrSe_6$ octahedra via common edges and faces results in a displacement of the Cr atoms from the centers of the octahedra and alternating short and long Cr–Cr distances are found. The resulting quasi-two-dimensional metal atom network is displayed in Fig. 1b. A single zigzag chain made up of Cr2 atoms runs parallel to the crystallographic *b* axis and double zigzag chains of Cr1 and Cr3 atoms are parallel to the (001) plane (Fig. 1b).

Tl-deintercalated samples can be prepared via a topotactic redox reaction of stoichiometric $TlCr_5Se_8$ using bromine in acetonitrile. Special attention was drawn to possible reaction paths and the question of whether Tl or the host lattice is oxidized during the reaction. We have

0022-4596/99 $30.00

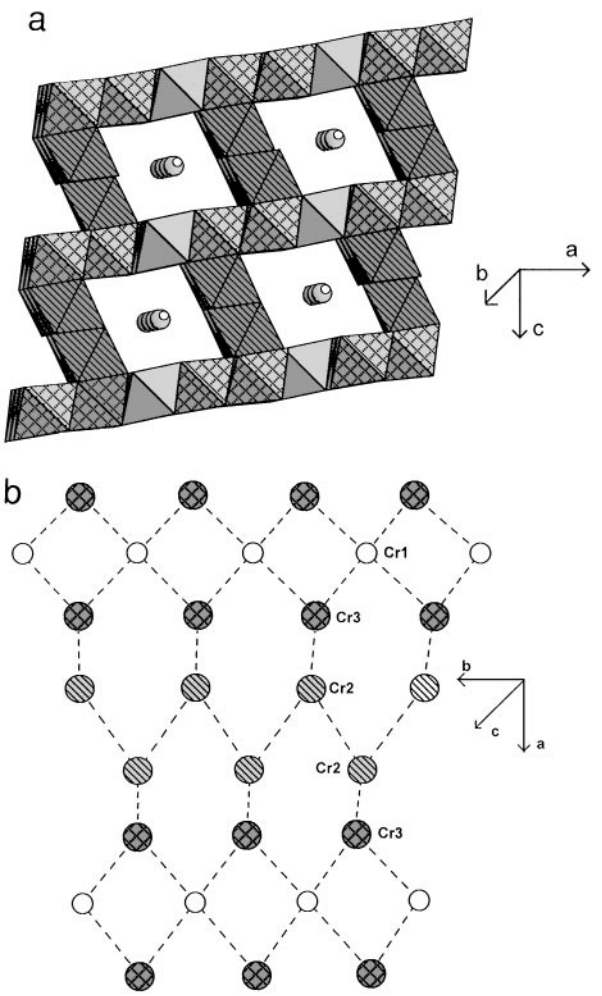

FIG. 1. (a) Polyhedral representation of the crystal structure of $TlCr_5Se_8$. The Cr2 centered octahedra are marked with lines, the Cr3 octahedra are cross hatched. (b) The quasi-two-dimensional metal atom network.

demonstrated that with decreasing Tl content the lattice parameters show a very anisotropic behavior, which is a direct consequence of the changes of the interatomic Cr–Cr separations. The strongest contraction was observed for the *a* axis. In contrast to the strong changes observed for the interatomic Cr–Cr distances the average Cr–Se as well as the nonbonding Se–Se separations were shown to be only slightly affected. The results of our experiments definitely excluded the formation of Tl^{3+} during the redox reaction but did not allow a definite decision on whether the chromium or selenium atoms are oxidized when Tl is removed.

More information on this subject can be expected from low-temperature X-ray investigations, magnetic susceptibility measurements, and EPR experiments. The magnetic properties of Tl-poor samples of $Tl_xCr_5Se_8$ should be different depending on whether Cr(III) is oxidized to Cr(IV) or Se(-II) is oxidized to Se(-I). In addition, the structural changes resulting from Tl deintercalation should affect the observed magnetic properties. Such considerations are based on Goodenough's and Kanamori's model qualitatively describing the competition between direct cation–cation and indirect cation–anion–cation exchange (2–4). The direct Cr^{3+}–Cr^{3+} interaction involves the half-filled t_{2g} levels of the Cr^{3+} ions, thus favoring an antiferromagnetic coupling of the spins. The analysis of the magnetic properties of a large number of chromium chalcogenide spinels revealed that the strength of the direct exchange interactions is only substantial below a critical distance R_c of about 3.5 Å (33). On the other hand, indirect 90° superexchange of the type Cr^{3+}–X^{2-}–Cr^{3+} involves a half-filled t_{2g} orbital of one cation, an empty e_g orbital of the second cation and a doubly occupied *p* orbital of the anion, thus favoring ferromagnetic exchange. With increasing deviation of the angle from 90° the ferromagnetic exchange becomes weaker. Both mechanisms can occur simultaneously and which type dominates strongly depends on the actual interatomic metal-to-metal distances and Cr–*X*–Cr angles.

Besides the exchange paths involving only Cr(III) centers, the interaction of Cr(IV) (d^2) with Cr(III) (d^3) should lead to ferromagnetic exchange interactions due to double exchange, and if Cr(IV) is formed during the topotactic redox reaction drastic changes in the magnetic properties are to be expected that cannot be explained within the framework of the above mentioned rules. A partial oxidation of the selenium anions, on the other hand, would lead to the formation of valence band holes, that are significantly influence the magnetic properties. It was demonstrated that such holes need not condensate forming *X*–*X* bonds (5–8). For copper chromium and silver chromium chalcogenide spinels of the type $CuCr_2X_4$ (X = S, Se, Te) and $AgCr_2Te_4$ (8), for example, the ferromagnetic Curie temperature strongly varies with the concentration of such holes (8) indicating that the strength of these interactions depends on the hole concentration in the valence band.

To this end, we here report on our results of X-ray, EPR, and magnetic susceptibility investigations performed on different $Tl_xCr_5Se_8$ samples. The structural changes as a function of temperature are discussed in relation with the observed magnetic properties.

EXPERIMENTAL

The samples were prepared according to the recipes given in Part I (1). Deintercalation experiments were performed with ground and sieved samples (mesh < 250). The homogeneity of the samples was checked with X-ray powder diffractometry and the compositon was determined using atomic absorption spectrometry (AAS). To get an impression of the compositional variation with respect to the Tl

content, Rietveld refinements were performed for selected samples using the program FULLPROF. The Rietveld refinement results obtained on stoichiometric $TlCr_5Se_8$ served as a standard for the widths of the reflections. Careful analysis of the reflection profiles gave no hints for an appreciable variation of the Tl abundance. The compositions derived from these refinements differed by $\delta = 0.03$ in $Tl_{x \pm \delta}Cr_5Se_8$ from those determined with AAS. The samples were also analyzed with EDX. Again no significant variation of Tl content was observed within the limits of the method.

Single crystals with a reduced Tl content were prepared in the following way. A Br_2/CH_3CN solution was heated every second day to about 50°C over a period of 6 weeks. After each heating cycle the solution was cooled to room temperature and held at this temperature for 1 day. Crystals prepared in this way were mechanically stable. The compositions of the crystals were determined during single-crystal structure refinements and the uncertainty of the Tl content was typically 0.02 (1). The absence of small amounts of water in the deintercalated samples was proved by TGA–DTA measurements up to 250°C.

Low-temperature single-crystal X-ray investigations were performed on a STOE AED II diffractometer (Mo$K\alpha$ radiation, $\lambda = 0.7107$ Å, Graphite monochromator) equipped with an Oxford Instruments Cryostream cooling device. The intensities were reduced to F_0 by Lorentz polarization corrections. A face-indexed absorption correction was also applied. All calculations were performed with the software SHELXTl PLUS (scattering factors for neutral atoms). Some important results of the refinements are summarized in Table 1. Lists of structure factors, interatomic angles, and anisotropic displacement parameters are available on request.

TABLE 1
Selected Informations of Data Acquisition and Refinement Results for $Tl_{0.32}Cr_5Se_8$

	T (K)				
	300	200	180	150	100
a (Å)	18.578(2)	18.500(2)	18.481(2)	18.444(3)	18.389(3)
b (Å)	3.5736(6)	3.5711(5)	3.5718(7)	3.5718(8)	3.5780(8)
c (Å)	8.898(1)	8.877(1)	8.876(2)	8.869(2)	8.875(2)
β (°)	104.00(1)	103.87(1)	103.81(1)	103.74(1)	103.55(1)
V (Å^3)	573.1(1)	569.4(1)	569.0(1)	567.6(1)	567.9(1)
$\sum I$	1225	1730	1173	2078	1995
Unique	958	950	952	944	943
Used ($I > 2\sigma(I)$)	680	721	688	711	715
R	0.0298	0.0308	0.0306	0.0348	0.0301
R_w	0.0311	0.0324	0.0318	0.0347	0.0317
$\Delta F(e^-/Å^3)$	2.55/−1.80	2.28/−2.37	1.92/−2.13	1.99/−2.3	2.27/−2.21

Note. The estimated standard deviations are given in parentheses. The number of refined parameters was 46.

Susceptibility measurements were conducted with a Faraday balance applying fields up to 0.9 T in the temperature range 4–300 K. Different samples were also measured with a Foner vibrating sample magnetometer at 1 T as well as with a SQUID device (Quantum Design, MPMS-7). Measurements with the SQUID were performed with applied fields of 100 G and 1000 G. All data were corrected for core diamagnetism using Pascal's increments. A zero-field cooling experiment was performed on one sample.

EPR spectra of $TlCr_5Se_8$ and $Tl_{0.45}Cr_5Se_8$ were recorded using a Bruker EMX-220 digital X-band spectrometer equipped with a Bruker ER 4121VT temperature control system at a $120(\pm 1) \leq T \leq 300(\pm 1)$ K interval. The $Tl_{0.45}Cr_5Se_8$ sample was selected because very close to this composition a transition from predominantly antiferromagnetic to ferromagnetic exchange was observed (see results and discussion).

For the measurements powdered samples were placed into glass capillary tubes centered into the rectangular cavity. For simultaneous precise measurements of g factor and signal intensity, several milligrams of a paramagnetic marker (DPPH, $g = 2.0036$) were introduced into the sample tube. Spectra were obtained with the following parameters: 9.4 GHz microwave frequency, 20 mW microwave power, 100 kHz and 2 G amplitude field modulation. Processing of the spectra (numerical integration, digital filtering, baseline correction, parameter calculation etc.) was performed using Bruker WIN-EPR Software.

RESULTS

Low-Temperature X-Ray Investigations

The evolution of the lattice parameters as a function of temperature for $Tl_{0.32}Cr_5Se_8$ and $Tl_{0.5}Cr_5Se_8$ is being displayed in Figs. 2 and 3, respectively. For both samples we observe a strong but not linear decrease in the a axis as well as in the monoclinic angle. The temperature dependence of both parameters exhibits a downward curvature. For $Tl_{0.32}Cr_5Se_8$ the c axis contracts down to about 150 K and shows hardly any change down to 100 K. For $x = 0.5$ the c axis passes a plateau between about 200 and 100 K and decreases again when the temperature is lowered to 80 K. The overall behavior of the c axis upon cooling is very similar for both compounds. In contrast, for both samples the b axis shows only minute changes down to 200 K, but increases steeply below 150 K. The increase between 180 and 100 K amounts to 0.0066 Å for $x = 0.32$ and 0.0061 Å for $x = 0.5$. The relative changes $\Delta b/b$ are 1.85×10^{-3} ($x = 0.32$) and 1.7×10^{-3} ($x = 0.5$), respectively.

A significant deviation of the unit cell volume from a linear behavior is observed at $T < 120$ K (see Fig. 4). For $Tl_{0.5}Cr_5Se_8$ the volume expansion between 120 and 80 K

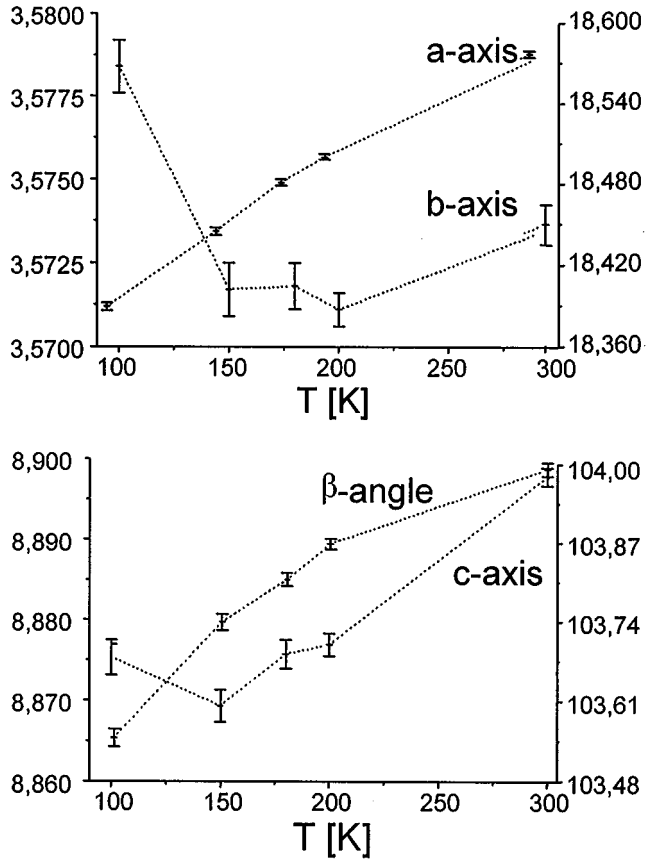

FIG. 2. Temperature dependence of the lattice parameters of $Tl_{0.32}Cr_5Se_8$. Units: Å for the axes and ° for the monoclinic angle. The dotted lines connecting the symbols serve as a guide for the eyes. The vertical bars represent the e.s.d.s obtained during lattice parameter refinements.

amounts to about 2 Å^3 and for $Tl_{0.32}Cr_5Se_8$ the volume expansion between 120 and 100 K amounts to 0.5 Å^3.

The variations of interatomic Cr–Cr distances in $Tl_{0.32}Cr_5Se_8$ as function of temperature are displayed in Fig. 5. The Cr1–Cr3 ($CrSe_6$ octahedra with common edge) and the Cr2–Cr3 (common face) distances decrease in a nearly linear fashion upon cooling. In contrast the Cr2–Cr2 separation (common edge) remains unchanged down to 200 K and starts to increase when the temperature is lowered further. Because the layers of Cr2-centered octahedra are running parallel to the crystallographic *b* axis, the increase of this axis is caused by the enlargement of the Cr2–Cr2 separation.

The changes of the interatomic Cr–Cr distances as a function of Tl content have been discussed in our previous contribution (1), but for a further discussion it is necessary to analyze variation of angles Cr^{3+}–Se^{2-}–Cr^{3+} near 90° as a function of Tl content (Figs. 6 and 7; for intralayer and interlayer definition see insets of Figs. 6 and 7). The intralayer angles Cr2–Se1–Cr2, Cr1–Se2–Cr3, and Cr1–Se4–Cr3 decrease from 90° toward smaller values from $x = 1$ to $x = 0.32$. For the Cr–Se–Cr interlayer angles a decrease with decreasing Tl content is observed and all angles become closer to 90°.

EPR Measurements

EPR spectra of powdered $TlCr_5Se_8$ show intense single broad asymmetric lines within the whole temperature range (Fig. 8a). No resolved fine or hyperfine structures were observed. At $T = 120$ K the broad Gaussian-like line is centered at high magnitude field ($g_{eff} = 1.850 \pm 0.005$). With increasing temperature it gradually changes to a narrower, but more asymmetric, line centered at lower field ($g_{eff} = 1.961 \pm 0.005$). EPR spectra of the Tl-poor $Tl_{0.45}Cr_5Se_8$ sample at room temperature consist of two weak, superimposed singlets with the broad and narrow lines being both centered in the same region ($g \sim 1.97$; Fig. 8b). With decreasing temperature, the broad line becomes more intense, narrows, and shifts toward low fields, whereas

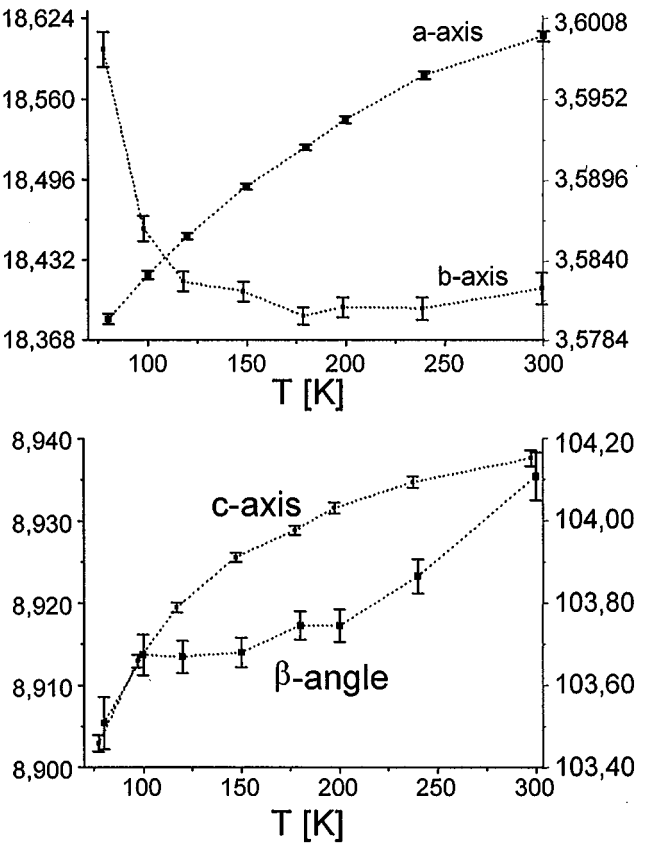

FIG. 3. Temperature dependence of the lattice parameters of $Tl_{0.5}Cr_5Se_8$. Units: Å for the axes and ° for the monoclinic angle. The dotted lines connecting the symbols serve as a guide for the eyes. The vertical bars represent the e.s.d.s obtained during lattice parameter refinements.

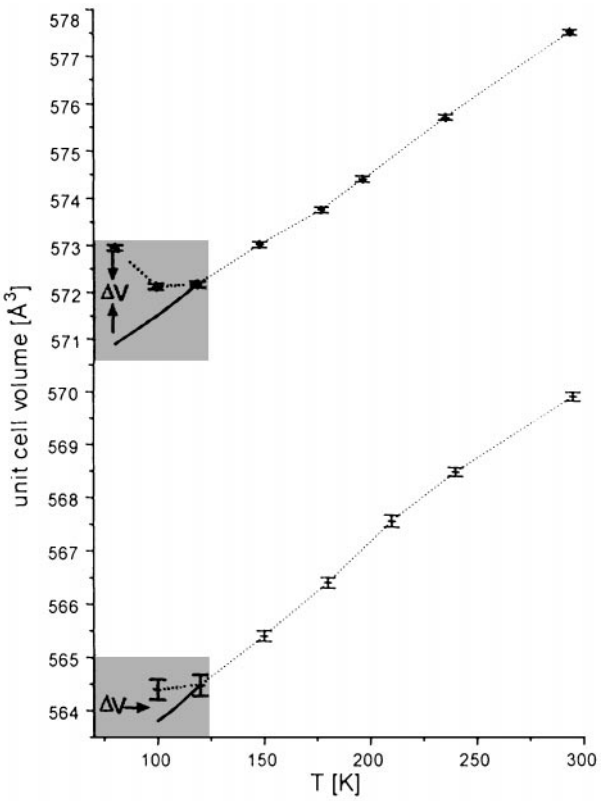

FIG. 4. Change of unit-cell volume Å^3 of $Tl_{0.32}Cr_5Se_8$ (bottom) and of $Tl_{0.5}Cr_5Se_8$ (top) as a function of temperature. The dashed line represents the experimental curve; the continuous line represents the linear extrapolated curve.

the narrow one remains at its place and disappears in the background of the strong broad line. However, at $T = 100$ K, where the intensity of the broad line drops significantly, the narrow line is recognized again.

The temperature variation of g_{eff} and the double integrated intensity (DI) are displayed in Figs. 9 and 10, respectively, for both samples. While the g factor of $TlCr_5Se_8$ only shows a slight increase from 1.8 at 100 K to 1.96 at room temperature (see above), a highly unusual temperature dependence is observed for the broad signal of $Tl_{0.45}Cr_5Se_8$: from a value of 2.28 at 100 K, the g factor first raises steeply to almost 2.5 at 130 K and then slowly drops to 1.97 at room temperature. In contrast, the g factor of the narrow signal is almost temperature-independent. The DI of the stoichiometric $TlCr_5Se_8$ sample slightly increases reaching the maximum at $T = 200 \pm 10$ K and then begins to decrease upon raising the temperature (Fig. 10, open circles). Crosses in Fig. 10 represent the temperature dependence of DI for the paramagnetic DPPH sample that was recorded simultaneously with the sample under study; as expected, DI for DPPH sample obeys the Curie law. In contrast, the temperature dependence of DI for the Tl-poor $Tl_{0.45}Cr_5Se_8$ sample shows a significant deviation from the Curie law (Fig. 10, solid circles): upon lowering the temperature, the DI passes through a maximum at $T = 130 \pm 5$ K and then sharply drops at lower temperatures. This behavior strongly resembles that of the g factor (see above).

Magnetic Measurements

The temperature dependence of the magnetic susceptibility of stoichiometric $TlCr_5Se_8$ is displayed in the inset of

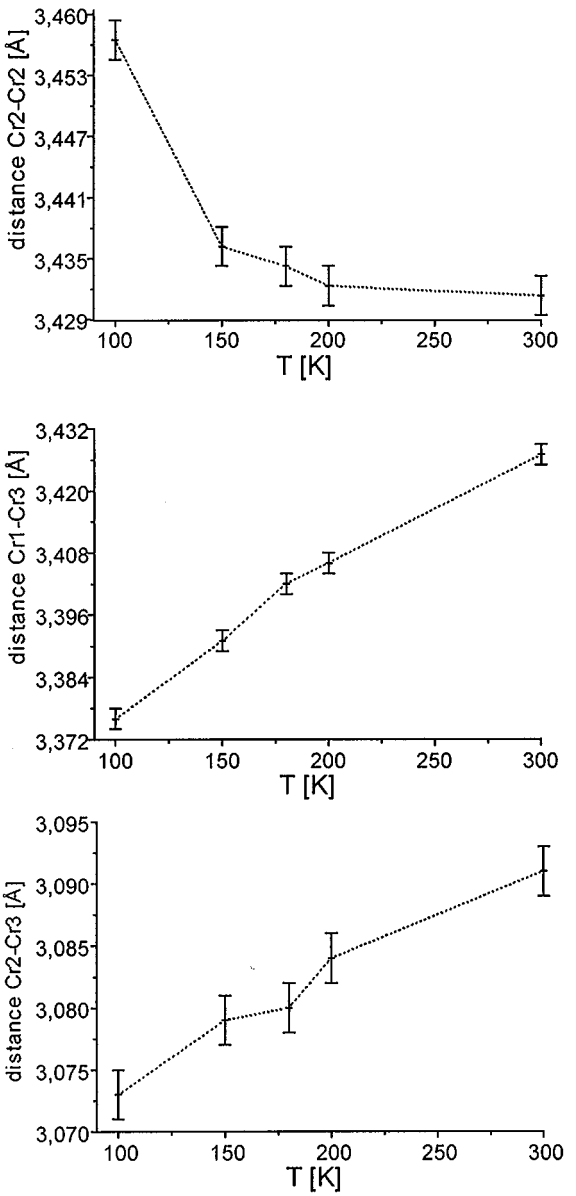

FIG. 5. Temperature dependence of the interatomic Cr–Cr distances Å in $Tl_{0.32}Cr_5Se_8$. The dotted lines connecting the symbols serve as a guide for the eyes. The vertical bars represent the e.s.d.s obtained at the end of the structure refinements. From top to bottom: Cr2–Cr2, Cr1–Cr3, Cr2–Cr3.

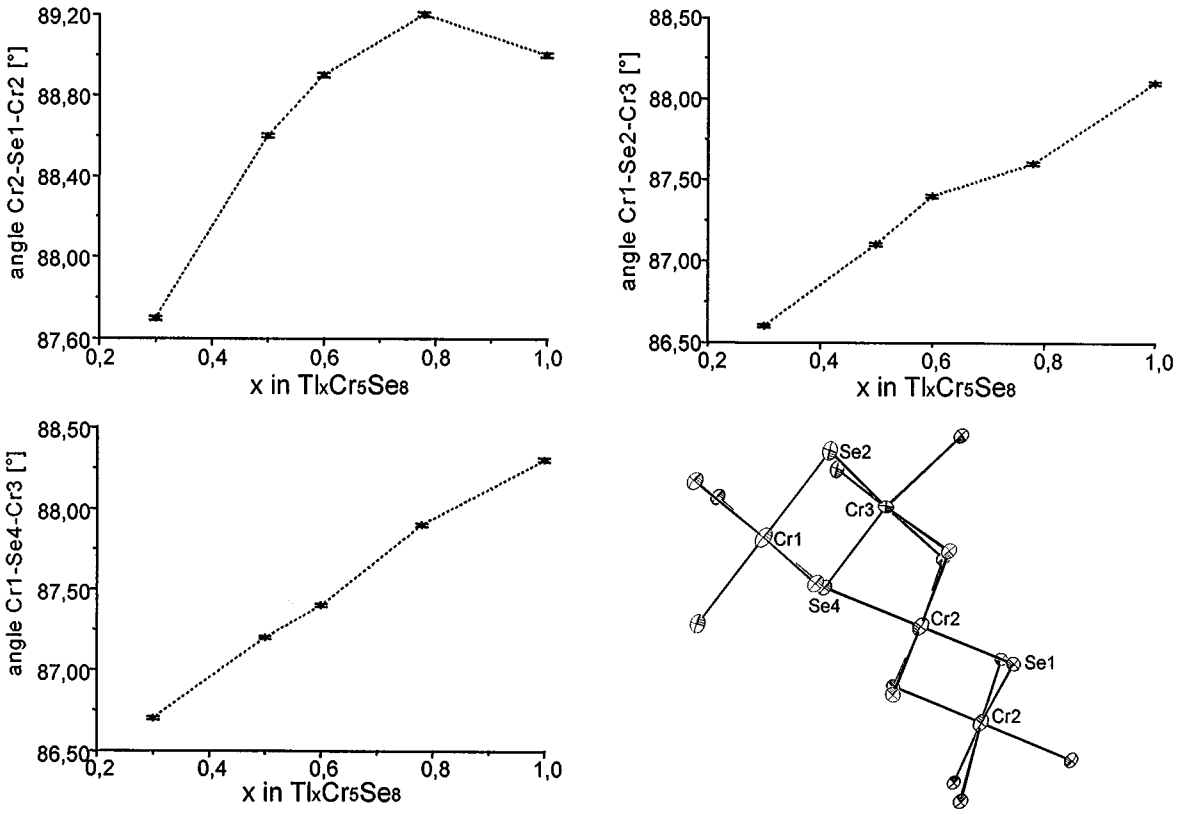

FIG. 6. Evolution of selected *intralayer* angles (°) as a function of Tl content in $Tl_xCr_5Se_8$. The dotted lines connecting the symbols serve as a guide for the eyes. The vertical bars represent the e.s.d.s obtained at the end of the structure refinements. Top left: Cr2–Se1–Cr2; top right: Cr1–Se2–Cr3; bottom left: Cr1–Se4–Cr3.

Fig. 11. With decreasing temperature the susceptibility increases passing a Néel point at about 55 K. Ohtani *et al.* reported a Néel temperature of 52 K (9, 10), in good agreement with our value for T_N. The high-temperature part of the susceptibility curve (200 to 300 K) was fitted with a Curie–Weiss law:

$$\chi(T) = C/(T - \theta).$$

The fitting procedure including a temperature-independent component from temperature-independent paramagnetism χ(TIP) resulting from delocalized electron density and diamagnetism gives a negative value for χ(TIP). This behavior is indicative of an antiferromagnetic ordering of localized magnetic moments and is in agreement with photoemission investigations demonstrating that $TlCr_5Se_8$ is a semiconductor (11, 12).

As expected extending the fitting range to lower temperatures yields slightly different values for C and θ without altering the overall trend.

The variation of the magnetic susceptibilities with the temperature of Tl-deintercalated samples ($x < 1$) (see Fig. 11) exhibits an unusual behavior: With decreasing temperature the susceptibilities pass through a maximum (χ_{max}) at about 125 K (T_{max}) and sharply drop to a value just below the value obtained at room temperature. Importantly, T_{max} is independent of x, but the values for χ_{max} strongly depend on the Tl content. However, no linear increase of χ_{max} with decreasing Tl content is observed: while the largest value of χ_{max} is obtained for a sample with the composition $Tl_{0.2}Cr_5Se_8$, the value for χ_{max} again drops significantly for the sample of nominal composition Cr_5Se_8. It is interesting that below about 90 K the magnetic susceptibilities are independent of composition, which is indicative of a similar spin arrangement for all samples with $x < 1$.

It must be stressed that the curves presented in Fig. 11 exhibit a totally different behavior from those published by Ohtani *et al.* (9). The reason for these remarkable differences is not clear, but can be due to different preparation methods of the Tl deintercalated samples. Ohtani *et al.* prepared $Tl_xCr_5Se_8$ by a topotactic redox reaction of $NaCr_5Se_8$ with an aqueous solution of $AlCl_3/FeCl_3$. They speculated that Na^+ was replaced by H_3O^+ during the reaction (9). In

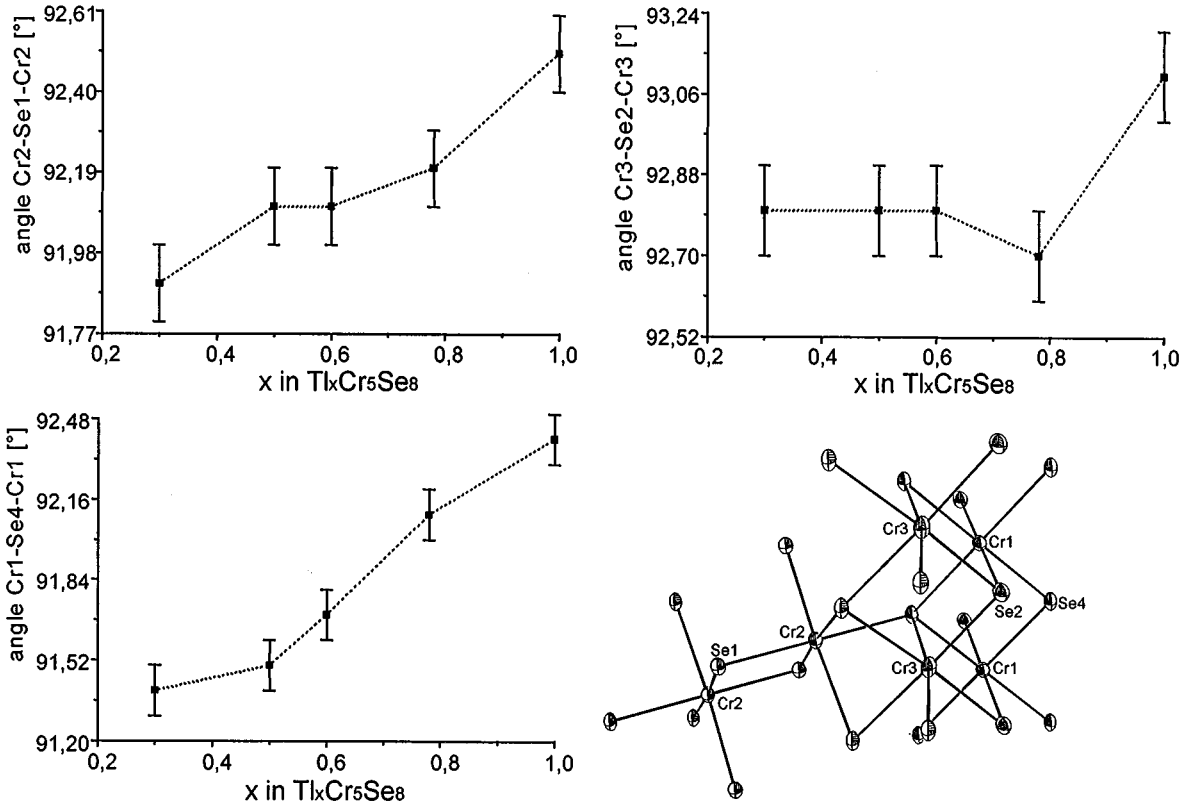

FIG. 7. Evolution of selected *interlayer* angles (°) as a function of Tl content in $Tl_xCr_5Se_8$. The dotted lines connecting the symbols serve as a guide for the eyes. The vertical bars represent the e.s.d.s obtained at the end of the structure refinements. Top left: Cr2–Se1–Cr2; top right: Cr3–Se2–Cr3; bottom left: Cr1–Se4–Cr1.

contrast, we can definitely exclude the presence of small amounts of water in our samples from TGA–DTA measurements.

The numerical results of the fits with the Curie–Weiss law are summarized in Table 2. In Table 3, magnetic data extracted from the literature are given for comparison. Remarkably, with decreasing Tl content the effective magnetic moment per Cr^{3+} decreases reaching a value of 3.61 μ_B/Cr^{3+} for the Tl-free sample that is significantly lower than the spin-only value for a d^3 spin system (see Fig. 12). However, if one assumes that one of the five Cr(III) atoms of the formula unit is oxidized to Cr(IV), an average theoretical spin-only moment of 3.63 μ_B is obtained, which is very close to the experimental value. This provides strong evidence for the assumption that the chromium and not the selenium atoms are oxidized upon Tl deintercalation. As can be seen in Table 2 and in Fig. 12 the effective magnetic moment per Cr atom does not decrease in a linear way. Several effects are responsible for this observation. As noted in the experimental section not all samples were measured on the same device. Furthermore, the actual compositions $Tl_{x\pm\delta}Cr_5Se_8$ can vary by $\delta = 0.03$, thus introducing a scatter of about ± 0.01 μ_B for the magnetic moment. It must be noted that the slight discrepancies do not change the actual trend observed and that the true μ_{eff} values are of less importance than the significant decrease of the effective magnetic moment with decreasing Tl content.

Importantly, the observed differences in the susceptibility curves of the Tl-deintercalated samples can be described with a variation in the Weiss constant θ. The evolution of θ as a function of Tl content is displayed in Fig. 12. For the stoichiometric sample the Weiss constant θ was estimated to be $-222(10)$ K indicative of pronounced antiferromagnetic exchange interactions (see above). This value is in good agreement with the values reported by Ohtani *et al.* (9, 10). However, when the Tl content is reduced to x just above 0.5 in $Tl_xCr_5Se_8$ the value for the Weiss constant θ steadily decreases, suggesting less strong antiferromagnetic exchange interactions. Further reduction of the Tl content results in a change of the sign of the Weiss constant, and for samples with $x < 0.5$ in $Tl_xCr_5Se_8$ a change of the sign for θ is observed. It must be stressed here that we investigated several samples with compositions near $x = 0.5$, and in all cases the values for the Weiss constant scattered around

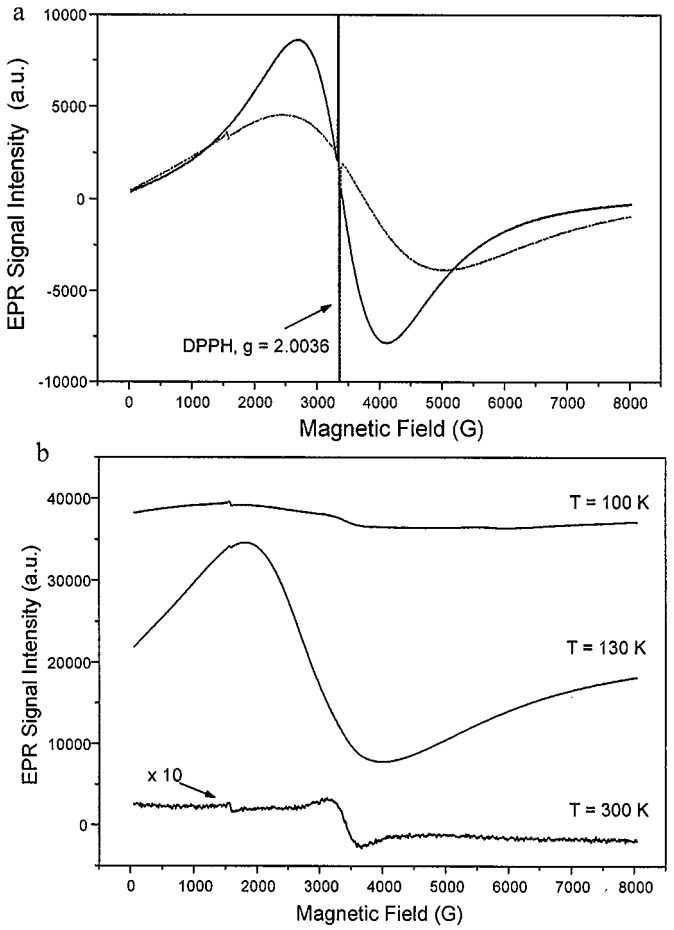

FIG. 8. EPR spectra of polycrystalline $TlCr_5Se_8$ (a) and $Tl_{0.45}Cr_5Se_8$ (b) at various temperatures, $\nu = 9.404$ GHz. Weak sharp peak at $g \sim 4.3$ (~ 1500 G) in all spectra belongs to Fe^{3+} impurity ions in the glass of the capillary tube.

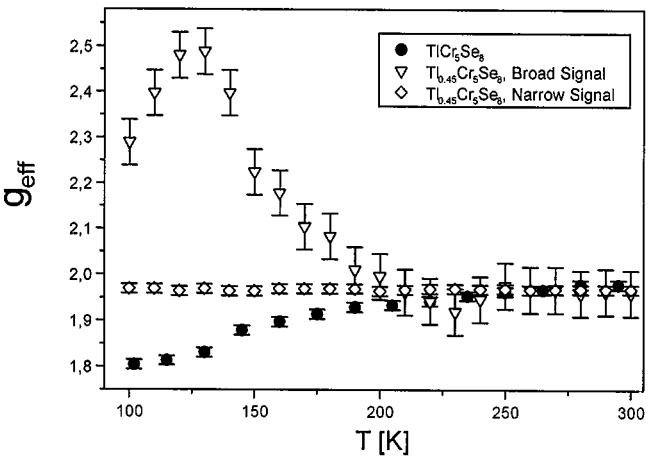

FIG. 9. Temperature dependence of g_{eff} for polycrystalline $TlCr_5Se_8$ (solid circles) and $Tl_{0.45}Cr_5Se_8$ (broad line, open triangles; narrow line, open diamonds).

0 K. The interpolation between the experimental values for θ shows that the change of the sign of θ in fact occurs near the composition $Tl_{0.5}Cr_5Se_8$; i.e., at this composition the formerly dominating antiferromagnetic exchange interactions alter to dominating ferromagnetic exchange. It is also noted that θ does not monotoneously increase with decreasing Tl abundance but reaches a maximum near the composition $x \approx 0.2$ (see above).

DISCUSSION

As in many binary and ternary chromium chalcogenides the occurrence of magnetic exchange interactions in $Tl_xCr_5Se_8$ is connected with an anomalous temperature dependence of the lattice parameters. Depending on the nature of the dominating exchange mechanism, an anomalous thermal expansion or contraction of the lattice parameters as well as of the unit cell volume has been reported (20–23) for ferromagnetic Cr_2Te_3 ($T_c = 180$ K) (23), for the ferrimagnetic compound Cr_2S_3 ($T_N = 130$ K) (26), and for ferromagnetic CrTe ($T_c = 331$–347 K) (22, 24, 25). For antiferromagnetic Cr_2Se_3 ($T_N = 43$ K) a sharp volume expansion was found at 40 K (23). The rhombohedral layer compound $Cr_2Ge_2Te_6$ is a ferromagnet ($T_c = 61$ K). Upon cooling the a axis linearly decreases, and below 100 K it starts to increase with falling temperature. The c axis contracts over the whole temperature range but shows a deviation from linear behavior at about 70 K (20).

In our samples the unit cell volumes of $Tl_{0.5}Cr_5Se_8$ and $Tl_{0.32}Cr_5Se_8$ exhibit an expansion upon cooling, starting near the temperature where the susceptibility passes through a maximum. Whereas the a and c axes as well as the

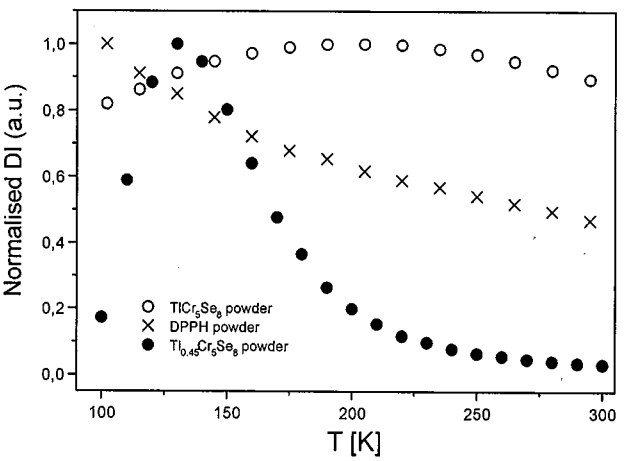

FIG. 10. Temperature dependence of normalized double intensity of EPR line for polycrystalline $TlCr_5Se_8$ (open circles) and $Tl_{0.45}Cr_5Se_8$ (solid circles) in comparison with DPPH (crosses).

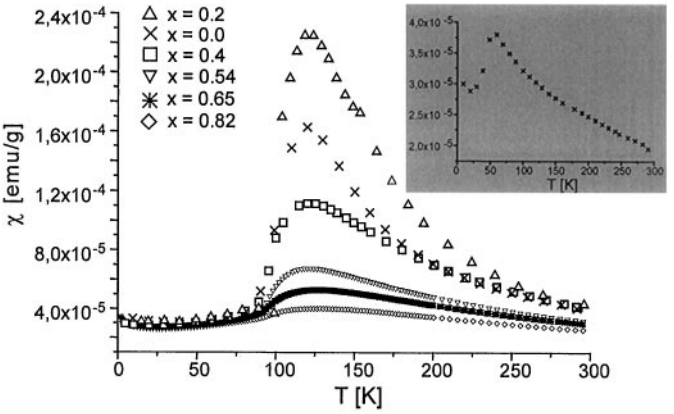

FIG. 11. Temperature dependence of the magnetic susceptibility of stoichiometric $TlCr_5Se_8$ (inset) and of Tl-deintercalated samples of $Tl_xCr_5Se_8$. Note the significantly different scaling of the susceptibility axes. Units: [emu/g].

monoclinic angle decrease in a nonlinear fashion upon cooling, the *b* axis starts to *increase* at about 200 K, exhibiting a sharp increase at about 120 K. Likewise the Cr1–Cr3 and Cr2–Cr3 distances are shortened with falling temperature, whereas the Cr2–Cr2 distance enlarges from 300 K down to 80 K with a sharp increase between 150 and 100 K, leading to the observed expansion of the *b* axis. This unusual behavior suggests that the positive charge associated with a possible formation of Cr(IV) is located on the Cr2 site when the temperature is lowered, thus leading to strong repulsions. At higher temperatures the additional charge moves between Cr2 and Cr3, thus lowering the repulsion between Cr2 and Cr2. We demonstrated in our previous contribution that with decreasing Tl content the Cr2–Cr3 distance (common face) was enlarged. This observation also suggests that at 300 K the additional positive charge moves between the Cr2 and Cr3 site. Within a simple ionic picture the oxidation of Cr(III) to Cr(IV) should lead to a smaller average Cr^{n+} radius ($r(Cr^{3+}) = 0.615$ Å and $r(Cr^{4+}) = 0.55$ Å). Assuming a constant radius for Se^{2-} the average ⟨Cr–Se⟩ bond length should be reduced by about 2.2% when *x* is lowered from 1 to about 0, but the measured changes of the ⟨Cr–Se⟩ distances are only of the order of 0.2%. However, our experimental results do not represent a contradiction to Cr(IV) formation as it is well known that for compounds with pronounced covalent bonds there exist no *unique* radii for the elements involved. On the other hand, a shortening of the average ⟨Cr–Se⟩ distances also should occur if Se^{-II} is partially oxidized to Se^{-I}. It is interesting to note that such a shortening of the Cr–Se bond by about 0.05 Å (equal to 1%) was reported for $Cu_2Cr_2Se_4$ when valence band holes are created by the removal of Cu. But a significant decrease of the *a* axis was also observed (7).

Formally, the thermal evolution of the magnetic susceptibilities is reminiscent of a spin-glass behavior, with an unusually high spin-glass transition temperature (13). However, because the magnetic susceptibilites of the different samples did not exhibit the typical field dependence of χ_{max} and a zero field cooling experiment showed a temperature dependence of the susceptibility nearly identical to that obtained during the normal procedure, we exclude this possibility.

The possible occurrence of a so-called magnetically quasi-ordered phase (MQO) also must be taken into account. The MQO results from the competition between a positive effective exchange integral J_+ and a negative one J_-. In the metallic dilute alloy system AuFe the origin of J_+ and J_- is ascribed to the indirect exchange interaction due to the conduction electrons (RKKY interaction) (14). There also exist examples for MQO in insulating systems like $Eu_xSr_{1-x}S$ (15, 16). The positive exchange J_+ results from the first-nearest-neighboring magnetic atoms Eu and J_- from the second-nearest-neighboring ones. These short distance interactions can be ascribed to direct and superexchange interactions. A MQO behavior was also reported for the system $(Cr_{1-y}V_y)_{1-d}$ ($d = 0.14$) with broad susceptibility maxima at temperatures between 40 and 50 K (17). It is noted, however, that the magnetic susceptibility curves of these samples show a characteristic dependence from field strength; i.e., the broad susceptibility maxima become sharper with decreasing field strength. Because we observed no such change in the shape and location of the susceptibility maximum at 125 K we also exclude the possibility of a MQO phase.

As mentioned in the Introduction, the Kanamori and Goodenough rules (2–4) often allow prediction of the type of

TABLE 2
The Effective Magnetic Moment per Cr Center and the Weiss Constant θ for $Tl_xCr_5Se_8$

	x									
	0	0.13	0.2	0.3	0.4	0.54	0.59	0.65	0.82	1
μ_{eff}/Cr (μ_B)	3.61(3)	3.70(2)	3.64(3)	3.78(5)	3.80(3)	3.79(3)	3.88(3)	3.87(3)	4.02(3)	4.14(5)
θ(K)	73(2)	96(2)	104(4)	80(4)	63(2)	7.4(2.4)	− 26(3)	− 35(3)	− 75(5)	− 222(10)

TABLE 3
Magnetic Data for Different Cr Chalcogenides Compiled from the Literature

Compound	θ(K)	$\mu_{eff}/Cr\,(\mu_B)$	χ(TIP) 10^{-6}(emu/g)	Ref.
$TlCr_5Se_8$	− 218	4.01	1.76	(10)
$InCr_5Se_{7.8}$	− 233	4.2	0.72	(10)
$KCr_5Se_{7.8}$	− 171	4.46	− 2.2	(10)
$TlCr_5Te_{7.8}$	70	2.65	—	(10)
$TlCr_5Se_8$	− 218	4.04	0.991	(9)
$Tl_{0.65}Cr_5Se_8$	− 207	3.69	3.13	(9)
$Tl_{0.33}Cr_5Se_8$	− 90.8	3.96	—	(9)
$TlCrS_2$	120	3.59	—	(27)
$TlCrSe_2$	130	3.71	—	(27)
$TlCrTe_2$	91	4.47	—	(27)
$TlCr_3S_5$	− 259	3.43	—	(27)
$TlCr_3Se_5$	− 156	2.79	—	(27)
$AgCrO_2$	− 211	3.96	—	(27)
$Cr_2Sn_3Se_7$	3.26	3.65	—	(13)
$V_{0.9}Cr_{0.1}Se$	− 1482	12.85	—	(28)
$V_{0.17}Cr_{0.83}Se$	48	3.74	—	(28)
$LaCrS_3$	− 390	3.9	—	(29)
$Gd_{2/3}Cr_2S_4$	8	—	—	(30)
$CrSbSe_3$	—	3.90	—	(31)
$CrSiTe_3$	—	3.58		(32)

coupling between transition metal ions as a function of the geometry of the structure. For a number of layered chromium chalcogenides and chromium spinels with CrX_6 octahedra (X = S,Se) connected by common edges ($Ag_{1/2}Cr_{1/2}PS_3$ and $ACrX_2$; A = K, Na, Ag, Cu, Li; X = S, Se; MCr_2X_4, M = Cd, Hg; X = S, Se), the parameter J/k for nearest neighbor (n.n.) exchange is negative for Cr–Cr = 3.38 Å and becomes positive at about 3.52 Å. This means that the sign of J/k is very sensitive to the interatomic Cr–Cr distance, since a 4% variation of this distance results in a change from weak ferromagnetism to strong antiferromagnetism (18, 42). It must be noted that the relationship between Cr–Cr separation and sign of the exchange parameter was developed for Cr(III) centers and for CrX_6 octahedra being connected via common edges. That this correlation does not work in every case even for Cr atoms in the oxidation state III was demonstrated for $Cu_{2x}Cr_{2x}Sn_{2-2x}S_4$ (43). The correlation J/k vs d(Cr–Cr) predicts an antiferromagnetic n.n. interaction in contrast to the observed ferromagnetic n.n. exchange (43).

Nevertheless, if only direct Cr^{3+}–Cr^{3+} or indirect Cr^{3+}–Se^{2-}–Cr^{3+} exchange interactions are considered for $Tl_xCr_5Se_8$, the following magnetic behavior can be expected. In the first step only the layers built by Cr1 and Cr3 and Cr2–Cr2 centered octahedra are taken into account: In stoichiometric $TlCr_5Se_8$ the Cr–Cr distances across common edges amount to 3.493 and 3.516 Å. These values are in the range where direct Cr–Cr exchange interactions should yield a weak ferromagnetism, i.e., a positive value for the Weiss constant. With decreasing Tl content these distances are significantly shortened reaching 3.427 and 3.431 Å at the composition $Tl_{0.32}Cr_5Se_8$. Assuming a similar trend as reported for the layered $ACrX_2$ compounds the decrease of about 2 and 2.5% should lead to strong antiferromagnetic exchange interactions, i.e., a change from the former weakly positive to negative θ values. The counteracting effect comes from indirect Cr^{3+}–Se^{2-}–Cr^{3+} superexchange. As noted above, the interlayer Cr–Se–Cr angles decrease with decreasing Tl content becoming closer to 90°. Hence, the antiferromagnetic exchange due to direct Cr^{3+}–Cr^{3+} interactions may be overcompensated by the stronger ferromagnetic superexchange, thus leading to a positive sign for θ. A ferromagnetic intralayer ordering together with a positive θ was reported for $NaCrSe_2$ with a long Cr–Cr distance of 3.73 Å and a Cr–Se–Cr angle of 93.5° (19). A positive paramagnetic temperature was also observed for orthorhombic

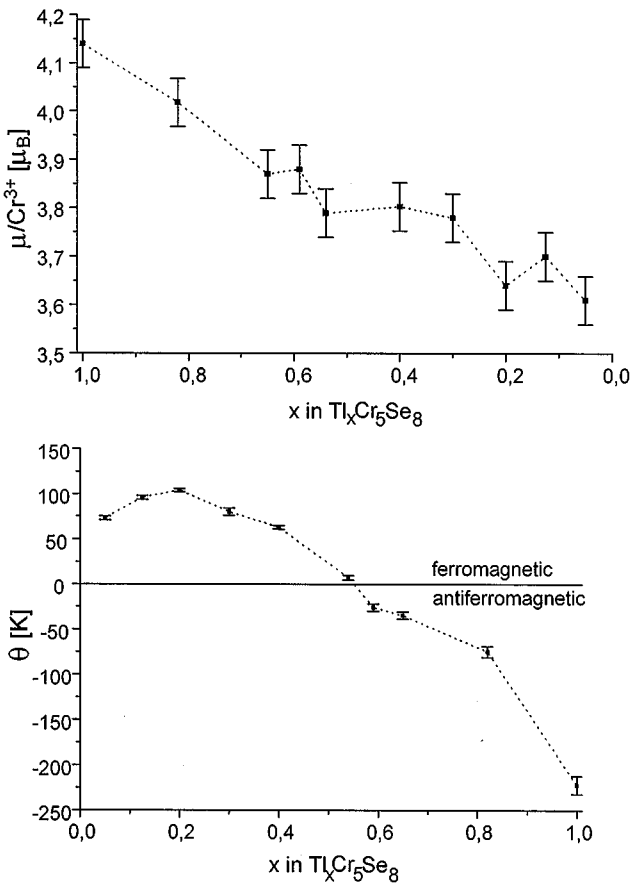

FIG. 12. (Top) Change of the effective magnetic moment per Cr^{3+} with Tl abundance in $Tl_xCr_5Se_8$. The dotted line serves as a guide for the eyes. (Bottom) Change of the Weiss constant θ with Tl content in $Tl_xCr_5Se_8$. The vertical line at $\theta = 0$ K represents the border between dominating antiferromagnetic and ferromagnetic exchange interactions. The dotted line serves as a guide for the eyes. The vertical bars represent the variations derived from the fitting procedure.

$Cr_2Sn_3Se_7$ with Cr–Cr distances ranging from 3.746(1) to 3.8307(2) Å and Cr–Se–Cr angles between 90.50(4) and 96.17(4)° (13). In both cases, however, the Cr–Cr interatomic separations are far too long for direct exchange, a situation quite different from the present samples. In the second step the connection of the layers via common faces must be considered, and the situation becomes more complex. The Cr2–Cr3 (common face) distance of 3.056 Å is short enough for strong antiferromagnetic exchange. This distance slightly increases to 3.091 Å when the Tl content is lowered to $x = 0.32$ in $Tl_xCr_5Se_8$, suggesting somewhat weaker antiferromagnetic interactions. What type of exchange is dominating cannot definitely be decided using a model with Cr^{3+} centers only, but the relatively short Cr–Cr distances in all $Tl_xCr_5Se_8$ samples as well as the small changes of the Cr–Se–Cr angles would suggest that the localized spins in all compounds are always *antiferromagnetically* ordered, in contrast to the experimental results.

To conclude, the only remaining explanation for the unusual magnetic properties is provided by the assumption that upon Tl deintercalation Cr(IV) centers are formed. Strong experimental evidences for this hypothesis are the decrease of the average effective magnetic moment per Cr being consistent with the formation of one Cr(IV) per formula unit in Tl-depleted $TlCr_5Se_8$ and the thermal evolution of the lattice parameters as correlated with changes in Cr–Cr distances indicating that the positive charge associated with the formation of Cr(IV) is localized at Cr2 at low temperatures and becomes delocalized between Cr2 and Cr3 at higher temperatures (see above). Below T_c, the existence of localized Cr(IV) centers gives rise to local ferromagnetic couplings which, however, amount to net antiferromagnetic behavior. Upon raising the temperature to T_c, the positive charge gets delocalized between Cr2 and Cr3 and thus larger *domains* of ferromagnetically coupled spins are created. The number of ferromagnetic interactions increases with increasing number of Cr(IV) centers (decreasing Tl content), which explains the change of dominating antiferromagnetic interactions in stoichiometric to dominating ferromagnetic interactions in Tl-deintercalated samples with $x < 0.5$ (see above).

The EPR results are in full agreement with the magnetic data and this interpretation. For the stoichiometric sample, both g_{eff} values (Fig. 9) and the unusual temperature dependence of DI (Fig. 10) are strong evidences that the EPR spectra observed cannot be described within the framework of single isolated Cr^{3+} ions ($S = 3/2, g = 1.97$–1.98) (34), but reflect antiferromagnetic interactions. The spectra of the Tl-deintercalated sample (Fig. 8b), on the other hand, may be described by a superposition of two non- (or weakly) interacting paramagnetic centers having different origin. The narrow line at $g = 1.97$ shows a temperature-independent g factor and linewidth. Although it is hard to determine within a wide temperature range, its temperature dependence appears to obey a Curie law. This line may be associated with a single uncoupled Cr^{3+} ion. In contrast, the broad EPR line shows an unusual temperature dependence. Its DI(T) curve (Fig. 10, solid circles) behaves in the same manner as $\chi(T)$; i.e., it has a sharp maximum at 140 K (cf. Fig. 11). Therefore, it may be concluded that the paramagnetic centers responsible for this signal produce the main contribution to the magnetic susceptibility. Another remarkable feature of this signal is the temperature dependence of the effective g factor (Fig. 9, open triangles). In contrast to the stoichiometric sample (Fig. 9, solid circles), g_{eff} follows the susceptibility curve, increasing toward lower temperatures with decreasing temperature and passing through the maximum at $T = 130$ K. The increase of g_{eff} at decreasing temperature reflects an increase in the local magnetic field due to a parallel alignment of neighboring spins caused by ferromagnetic interactions. Likewise the sharp drop of both DI and g_{eff} below $T = 130$ K is due to 3D antiferromagnetic coupling induced by the localization of the Cr(IV) centers which was also evident from the structural and magnetic susceptibility data (see above). In summary, the unusual temperature and composition dependence of the susceptibility and EPR data can be traced back to competing antiferro- and ferromagnetic interactions, the latter depending upon the number of Cr(IV) centers produced by Tl deintercalation. Thus, $TlCr_5Se_8$ represents a system in which the magnetic properties are tunable over a wide range by a simple and fully controllable chemical modification.

In a further contribution we will report on the results of our photoemission investigations. The XPS/UPS experiments prove that the oxidation reaction in fact takes place in the host matrix, i.e., that chromium is oxidized from Cr(III) to the unusual Cr(IV) charge state.

ACKNOWLEDGMENTS

Financial support by the Deutsche Forschungsgemeinschaft (DFG) as well as by the Fonds der Chemischen Industrie is gratefully acknowledged. It is a pleasure to thank Dr. R. Kremer (Max-Planck-Institut Stuttgart) for some of the magnetic susceptibility measurements.

REFERENCES

1. W. Bensch, O. Helmer, and C. Näther, *J. Solid State Chem.* **127,** 40 (1996).
2. J. B. Goodenough, *J. Phys. Chem. Solids* **6,** 287 (1958).
3. J. B. Goodenough, *J. Phys. Rev.* **100,** 564 (1955).
4. J. Kanamori, *J. Phys. Chem. Solids* **10,** 87 (1959).
5. A. Payer, M. Schmalz, W. Paulus, R. Schöllhorn, R. Schlögl, and C. Ritter, *J. Solid State Chem.* **98,** 71 (1992).
6. A. Payer, M. Schmalz, R. Schöllhorn, R. Schlögl, and C. Ritter, *Mater. Res. Bull.* **25,** 515 (1990).
7. A. Payer, R. Schöllhorn, C. Ritter, and W. Paulus, *J. Alloys Comp.* **191,** 37 (1993).

8. A. Payer, A. Kamlowski, and R. Schöllhorn, *J. Alloys Comp.* **185,** 89 (1992).
9. T. Ohtani, Y. Sano, K. Kodama, S. Onoue, and H. Nishihara, *Mater. Res. Bull.* **28,** 501 (1993).
10. T. Ohtani and S. Onoue, *Mater. Res. Bull.* **21,** 69 (1986).
11. W.Bensch, E. Wörner, and P. Hug, *Solid State Commun.* **86,** 165 (1993).
12. W. Bensch, O. Helmer, C. Näther, and M. Muhler, *J. Solid State Chem.* **145,** 247 (1999).
13. S. Jobic, F. Bodenan, G. Ouvrard, E. Elkaim, and J. P. Lauriat, *J. Solid State Chem.* **115,** 165 (1995).
14. B. R. Coles, B. V. B. Sarkissian, and R. H. Taylor, *Philos. Mag.* **37,** 489 (1978).
15. H. Maletta and W. Felsch, *Phys. Rev.* **B20,** 1245 (1979).
16. K. Binder, W. Kinzel, and D. Stauffer, *Z. Phys.* **B36,** 161 (1979).
17. S. Ohta, S. Kurosawa, and S. Anzai, *J. Phys. Soc. Jpn.* **51,** 1386 (1981).
18. P. Colombet and L. Trichet, *Solid State Commun.* **45,** 317 (1983).
19. F. M. R. Engelsmann, G. A. Wiegers, F. Jellinek, and B. Van Laar, *J. Solid State Chem.* **6,** 574 (1973).
20. V. Carteaux, D. Brunet, G. Ouvrard, and G. Andre, *J. Phys.: Condens. Matter* **7,** 69 (1995).
21. M. Yuzuri, M. Narita, T. Kaneko, S. Abe, and H. Yoshida, *J. Phys.* **Coll. C8,** Suppl. 12, 233 (1988).
22. S. Ohta, T. Kanomata, T. Kaneko, and H. Yoshida, *J. Phys.: Condens. Matter* **5,** 2759 (1993).
23. S. Ohta, Y. Adachi, T. Kaneko, M. Yuzuri, and H. Yoshida, *J. Phys. Soc. Jpn.* **63,** 2225 (1994).
24. V. A. Gordienko, V. V. Zubenko, and V. I. Nikolaev, *Soviet Phys. JETP* **30,** 864 (1970).
25. H. Ido, K. Shirakawa, T. Suzuki, and T. Kaneko, *J. Phys. Soc. Jpn.* **26,** 663 (1969).
26. M. Yuzuri, T. Kanomata, and T. Kaneko, *J. Magn. Magn. Mater.* **70,** 223 (1987).
27. M. Rosenberg, A. Knülle, H. Sabrowsky, and Chr. Platte, *J. Phys. Chem. Solids* **43,** 87 (1982).
28. S. Yuri, S. Ohta, S. Anzai, M. Aikawa, and K. Hatakeyama, *J. Magn. Magn. Mater.* **70,** 215 (1987).
29. A. Lafond, A. Meerschaut, J. Rouxel, J. L. Tholence, and A. Sulpice, *Phys. Rev. B* **52,** 1112 (1995).
30. A. Meerschaut, A. Lafond, L. M. Hoistad, and J. Rouxel, *J. Solid State Chem.* **111,** 276 (1994).
31. D. Odink, V. Carteaux, C. Payen, and G. Ouvrard, *Chem. Mater.* **5,** 237 (1993).
32. R. E. Marsh, *J. Solid State Chem.* **77,** 190 (1988).
33. R. J. Bouchard, P. A. Russo, and A. Wold, *Inorg. Chem.* **4,** 685 (1965).
34. J. R. Pilbrow, "Transition Ion Electron Paramagnetic Resonance," Clarendon Press, Oxford, 1990.
35. J. Lakshmana, B. Sreedhar, M. Ramachandra Reddy, and S. V. J. Lakshman, *J. Non-Cryst. Solids* **111,** 228 (1989).
36. J. Srinivasa Rao, J. Lakshmana Rao, and S.V. J. Lakshman, *Solid State Commun.* **85,** 529 (1993).
37. D. E. Bolster, P. Gütlich, W. E. Hatfield, S. Kremer, and E. W. Müller, *Inorg. Chem.* **22,** 1725 (1983).
38. J. T. Veal, W. E. Hatfield, D. Y. Jeter, J. C. Hempel, and D. J. Hodgson, *Inorg. Chem.* **12,** 342 (1973).
39. R. L. Carlin, "Magnetochemistry," Springer-Verlag, Berlin/Heidelberg/New York/Tokyo, 1986.
40. W. Bensch, E. Wörner, M. Muhler, and U. Ruschewitz, *J. Solid State Chem.* **110,** 234 (1994).
41. P. D. Krasicky, J. C. Scott, R. H. Silsbee, and A. L. Retter, *J. Phys. Chem. Solids* **39,** 991 (1978).
42. P. Colombet and M. Danot, *Solid State Commun.* **45,** 311 (1983).
43. P. Colombet, M. Danot, and J. L. Soubeyroux, *J. Magn. Magn. Mater.* **51,** 257 (1985).